Fermi Surface of Thallium: Radio-Frequency Size Effect*

C. A. Gage and R. G. Goodrich
Department of Physics and Astronomy, Louisiana State University
Baton Rouge, Louisiana 70803
(Received 7 December 1970)

Radio-frequency size-effect measurements were made on high-purity single-crystal thallium plates approximately 0.1–0.25 mm thick. Extremal calipers of the Fermi surface obtained from the data were self-consistently fitted with a Fermi-surface model consisting of a third-band hole surface and fourth- and fifth-band electron surfaces. The Fermi-surface model developed from the data is appreciably different from either the free-electron model or the model arising from a previous energy-band calculation. In particular, no calipers were observed that could be assigned to pockets of third-band holes at the M point in the Brillouin zone. The fourth-band electron hexagonal network is found to be considerably distorted from the free-electron model, with no connection along the ΓA direction and no pockets in the ΓMK plane. Comparisons between the present model and recent de Haas–van Alphen measurements are made.

I. INTRODUCTION

In the past, the Fermi surface (FS) of thallium has been investigated through magnetoresistance measurements,[1–5] the magnetoacoustic effect,[6–8] cyclotron resonance,[9,10] and the de Haas–van Alphen (dHvA) effect.[11–15] The results of these experiments have been interpreted in terms of the single-orthogonalized-plane-wave (OPW) model of the FS and on a FS model developed from a relativistic OPW (ROPW) energy-band calculation by Soven.[16] The agreement between these measurements and the two FS models is at best only fair. The present investigation was performed in order to obtain extensive and detailed dimensions of the Tl FS from which an accurate model could be developed. The major result of this experiment is an internally consistent model of the FS which displays general agreement with past experiments.

The determination of FS dimensions using the radio-frequency size effect (RFSE) has been described in detail earlier.[17,18] In the RFSE experiment, a thin single-crystal plate of the sample is placed in a magnetic field parallel to its surface. Discontinuities in the rf surface impedance of the sample are exhibited when the strength of the magnetic field is such that extremal electronic orbits on the FS exactly span the sample thickness. The extremal FS dimensions are then obtained from the relation $k_c = 0.015194Hd$, where H is the value of the applied field in G at the point where the extremal orbits just span the sample, d is the sample thickness in mm, and k_c is the FS extremal dimension in Å^{-1}.

In the sections which follow, an explication of the experimental technique relevant to RFSE in thallium is presented, a presentation of experimental results, and, finally, the data analysis and caliper assignments are given.

II. EXPERIMENTAL PROCEDURE

The samples used in this experiment were cut from a zone-refined thallium bar (purity of 99.9999%) procured from Cominco Products Inc. The Tl bar contained crystals of sufficient size to facilitate sample preparation without further treatment. Large crystals cut from this bar had a resistance ratio $R_{4.2}/R_{300^\circ\text{K}}$ of ~5000. After orienting the selected crystals, thin slabs were cut from the bar with an acid string saw using a 60% acetic acid and 40% hydrogen peroxide solution. The general technique for RFSE sample preparation has been described in detail in Ref. 17. After spark planing, the samples were lapped in a solution of 40% acetic acid, 10% hydrogen peroxide, and 50% water to remove the surface strain caused by the thinning process and then stored in glycerine to avoid oxidation. The final sample thicknesses were typically between 0.1 and 0.25 mm. Samples this thin were necessary so that most of the calipers could be obtained at field strengths well above the superconducting critical field of ~95 G at 1.2 °K. Since thallium plates of this thickness are extremely susceptible to strain, it was necessary to prefabricate the rf oscillator tank coils. The samples were first washed in H_2O to remove the glycerine, then inserted in the preformed tank coil, and immediately placed in an evacuated Dewar for 24 h at 300 °K to remove all traces of the H_2O. In order to circumvent the possibility of strain during these operations, the sample thickness was not measured, nor was it rechecked for orientation until the experiment was completed. Laue back-reflection x-ray pictures showed that the sample orientation was always within ±0.5° of the desired direction after the RFSE measurements. The average sample thickness was determined by measuring the area of the face of the sample and

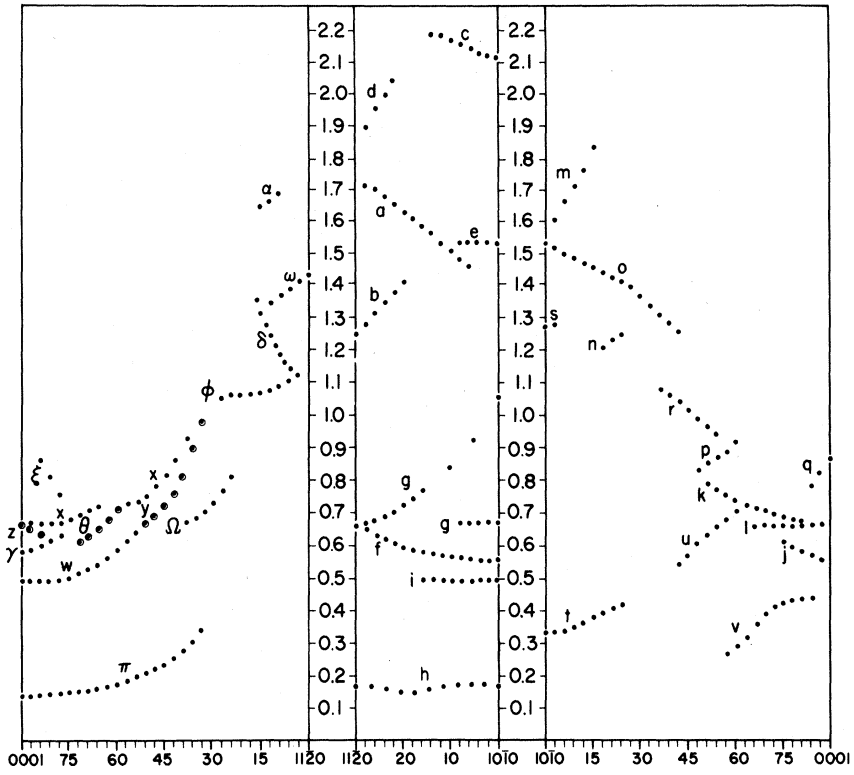

FIG. 1. Observed RFSE caliper values and caliper directions in the three principal planes of thallium. All calipers are measured in units of Å^{-1}.

weighing it in the manner described in Ref. 17. The RFSE signals were detected using the apparatus described in Ref. 18. Both the first and second derivatives of the real part of the surface impedance versus magnetic field can be recorded with this apparatus. The present measurements were performed at rf frequencies ranging from 5 to 10 MHz. The exact rf frequency used in each run was chosen to optimize the sensitivity of the marginal oscillator for the particular tank coil and sample being used. The method of recording the data combined with the sample thickness measuring technique gave an over-all reproducibility to the caliper values of 0.5%. This is the same reproducibility that was obtained in[18] Zn and is determined by comparing the caliper values of the same orbit on different samples.

III. EXPERIMENTAL RESULTS

Figure 1 is a plot of the FS calipers obtained for magnetic field rotations in the plane of the Tl plates having a normal $\vec{n}$ parallel to the [0001], [10$\bar{1}$0], and [11$\bar{2}$0] symmetry axes. Calipers that could be definitely identified as resulting from the addition of orbits are not shown.

The RFSE line shapes observed in Tl display the same general characteristics observed earlier in Cd[17] and Zn.[18] Of the more than fifty samples prepared, many exhibited rather weak RFSE signals. The reason for the low signal intensity in many of the samples is that the thin samples were extremely susceptible to strain which decreases the mean free path of the carriers. Signal strengths decreased rapidly with increased temperature, and the characteristic RFSE line shapes were not discernible on any of the samples above the superconducting transition temperature of Tl at 2.2 °K. Consequently, some of the orbits associated with smallest segments of the FS expected at low magnetic fields may not have been observed. The intensity of the RFSE signals is also dependent upon the geometry of the orbit. This fact aids in the caliper assignment and will be discussed in Sec. IV.

All of the caliper values reported here were calculated by choosing the point in field of maximum slope preceding the first major peak in the RFSE line shape obtained on a plot of the derivative of the real part of the surface impedance with respect to the magnetic field dR/dH. This point corresponds to the first peak in the second-derivative curve d^2R/dH^2. This has been shown to be a reliable point on the line shape from which to compute the caliper value in past RFSE experiments devoted to FS determinations.[17,18] In angular regions where many caliper series are present and the RFSE lines overlap, a slightly different procedure was used to determine the caliper point on each line. It was observed that the difference in field values between peaks on the second-derivative curves

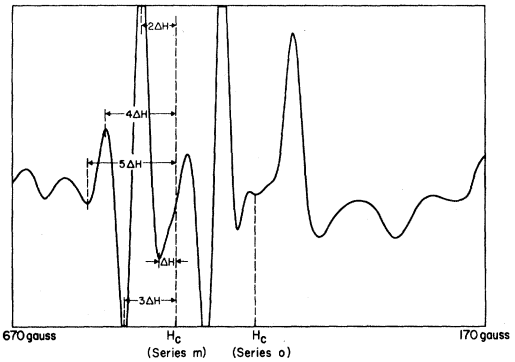

FIG. 2. Recorder tracing of d^2R/dH^2 vs H from 170 to 670 G with sample normal $\parallel [11\bar{2}0]$. The magnetic field is applied 9° from the [0001] direction.

ΔH was a constant for a given line. In Fig. 2 a recorder tracing of d^2R/dH^2 vs H taken with $\vec{H}$ applied 12° from [0001] direction in an $\vec{n} \parallel [11\bar{2}0]$ sample is shown. The line shapes associated with series m and o are shown on this plot. It is seen that ΔH is a constant for each line and the caliper point can be determined by extrapolating to the first peak in the line shape. This procedure was applied to determine the caliper values reported here even when the first peak in the second derivative was observable. In the latter cases, the extrapolated position of the first peak and the measured position agreed to within the measuring accuracy. The experimental error in the determination of the calipers by this method is ± 0.008 Å^{-1} for all but two caliper series which were always weak and could only be determined to ± 0.02 Å^{-1}. This accuracy was checked by comparing the caliper values obtained from different samples for the same orbit and by comparing the determination of points of the FS obtained from different sample orientations. These independent determinations always agreed to within the quoted accuracy. Since the third and fourth bands of Tl are degenerate along the AL line in the Brillouin zone (BZ), the calipers of the third- and fourth-band sheets in this direction should add to give the BZ dimension from L to L. As can be seen from Table I and the dimensions of the BZ given in the caption of Fig. 3, the agreement is within the quoted experimental error when the caliper point on the RFSE line is chosen in the manner described above. This point on the line has also been shown to be the caliper point for cylindrical Fermi surfaces in a recent calculation of line shapes by Juras.[19] Further support for the choice of this point on the line as the caliper point has recently been given by Boudreau and Goodrich[20] from line-shape studies on Cd.

IV. DATA ANALYSIS AND CALIPER ASSIGNMENT

In the following discussion, the term caliper will be construed to mean an extremal (maximum or minimum length) caliper in the direction of $\vec{n}\times\vec{H}$ with a magnitude equal to the projection of an extremal orbit in k space onto a plane perpendicular to $\vec{n}$. There are three types of orbits that give rise to the observed RFSE calipers: (i) orbits having true maximal or minimal extent in the $\vec{n}\times\vec{H}$ direction, (ii) truncated orbits which are orbits in a plane perpendicular to H that increase in extent until they no longer exist in the same form, and (iii) broken orbits which give rise to calipers between two turning points of an orbit on the FS (in this case the carriers do not complete a closed orbit before being scattered at the sample surface).[21] All three types of calipers have been reported previously[16,17] and were also observed in the present investigation. Table II lists the caliper series according to the type of orbit responsible for each series.

The BZ for Tl is illustrated in Fig. 3 with the dimensions along the symmetry directions indicated in the caption. The interpretation of the data is in terms of a FS having a third-band hole surface centered at A, a fourth-band electron hexagonal

TABLE I. FS dimensions of Tl along symmetry directions.

Direction	Band	Extremal calipers (Å^{-1}) Measured				Calculated	
		This experiment	Rayne	Eckstein	Coon	Soven	Free electron
$A\Gamma$	3	0.50		0.52	0.50	0.49	0.52
HK	4	0.49			0.51		
HK	5	0.44					
LM	4	0.67			0.67	0.64	
AL	3	1.43	1.46	1.43	1.47	1.44	1.55
AL	4	0.67	0.62		0.61	0.64	
AH	3	1.73	1.66	1.81	1.75	1.81	1.92
AH	4	0.67	0.64		0.72	0.62	
AH	4[a]	1.80				1.91	

[a]Dimension of the inside of the fourth-band electron hexagonal network in ALH direction.

network around the third-band hole surface in the *ALH* plane, and a fifth-band electron surface centered at *H*. No evidence exists from the present data that either the third band or the fourth band crosses the Fermi level along the ΓM direction or that the fourth band is connected to the adjacent BZ by posts lying in the ΓAHK plane. As will be discussed later, the results of this investigation and recent dHvA experiments suggest that these posts do not extend as high as the top of the fourth zone along *HK*. Extremal cross-sectional areas for the various orientations were calculated numerically directly from the measured calipers in cases where a true cross section is obtained (for instance, the third zone in the *ALH* plane). In the absence of central calipers which give the radii directly, the dimensions used in the area calculations were taken from scaled drawings constructed from the data. In Figs. 4–6 the solid lines represent the cross section of the FS in the respective planes, the dashed lines represent the projection of the extremities of the FS onto these planes, and the dotted lines are estimated connections between the experimentally determined sections of the FS. Also, in Fig. 6 an extremal-orbit outline on the FS is shown which was obtained by using all three symmetry plane projections to construct a cross-sectional view of the FS in a plane parallel to the *ALM* plane at a distance of 0.43 Å^{-1} along *AH*.

A. Third-Band Holes

Caliper series *a* was readily assignable as being due to minimal central orbits around the third-zone hole surface as indicated in Fig. 4. This series is very weak at angles less than 10° and not observed at all within 5° of the $[10\bar{1}0]$ axes due to the degeneracy existing between the third and fourth bands along the *AL* line.[22] The assignment of series *a* completely determines the outline of the third band in the *ALH* plane. Series *e* confirms the outline given by series *a* and is due to a noncentral maximum closed orbit (Fig. 3). Series *e* has been observed and assigned to the same noncentral orbit by Coon *et al.*[8] Series *b* arises from an inflection point in a plot of calipers versus distance along the direction of $\vec{H}$, k_H. At each angle of the applied field, a plot of the dimension of the *ALH* cross section perpendicular to k_H versus distance along k_H from the central orbit plane was made. Each of these curves shows a point of minimum slope (inflection point) at some value of k_H. Series *b* always fit the value of the caliper at the point of inflection. Orbits spanning both the third and fourth bands and passing through these degeneracy points were observed in all three orientations. Such orbits are represented in Figs. 4–6 (labeled *c*, α, and *n*, respectively). The corresponding dHvA area for the cross section of the third-zone surface in the *ALH* plane was calculated and is in excellent agreement with prior experiments (Table III).

TABLE II. Identification of the type of orbit responsible for the observed caliper series.

Type of orbit	Series
1 maximum or minimum	*acdefghjklmopqvwxyz*$\alpha\theta\xi\gamma$
2 truncated	*bstu*$\delta\Omega$
3 broken	*inr*$\pi\phi\omega$

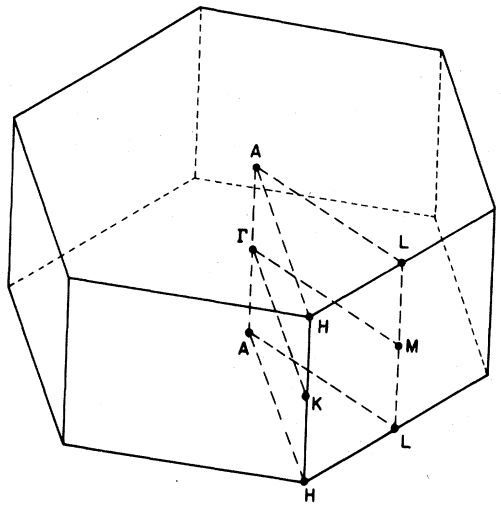

FIG. 3. Brillouin zone for hexagonal-close-packed thallium. The dimensions of the zone are $|\Gamma A| = 0.5735$ Å^{-1}, $|\Gamma M| = 1.0551$ Å^{-1}, and $|\Gamma K| = 1.2182$ Å^{-1}.

The assignment of series *o* and *p* to central maxima calipers on the projection of the third-band surface in the *ALM* plane implies that neither Soven's ROPW nor the single-OPW models accurately predicted the topology of the Tl FS. Series *o* and *p* indicate that the maximum distance that the central third-band hole surface extends parallel to the $A\Gamma$ direction is 0.44 Å^{-1} directly above a point 0.40 Å^{-1} from *A* towards *L* (Fig. 5). The further assignment of series *p*, *n*, *t*, *s*, *r*, *u*, ω, π, ϕ, γ, ξ, θ, α, Ω, and δ (Figs. 4 and 5) gives a completely consistent model for the third-band hole surface. The resultant model is shown schematically in Fig. 7. It has 12 projections parallel to the $A\Gamma$ direction—six major ones in the *ALM* planes and six minor ones in the *AHK* planes. The minor projections extend 0.35 Å^{-1} parallel to the $A\Gamma$ direction above a point 0.50 Å^{-1} from *A* towards *H*.

In addition to requiring that the model developed from the calipers be topologically consistent, the intensity of the RFSE peaks corroborate the assignment of caliper series. The intensity of the peaks

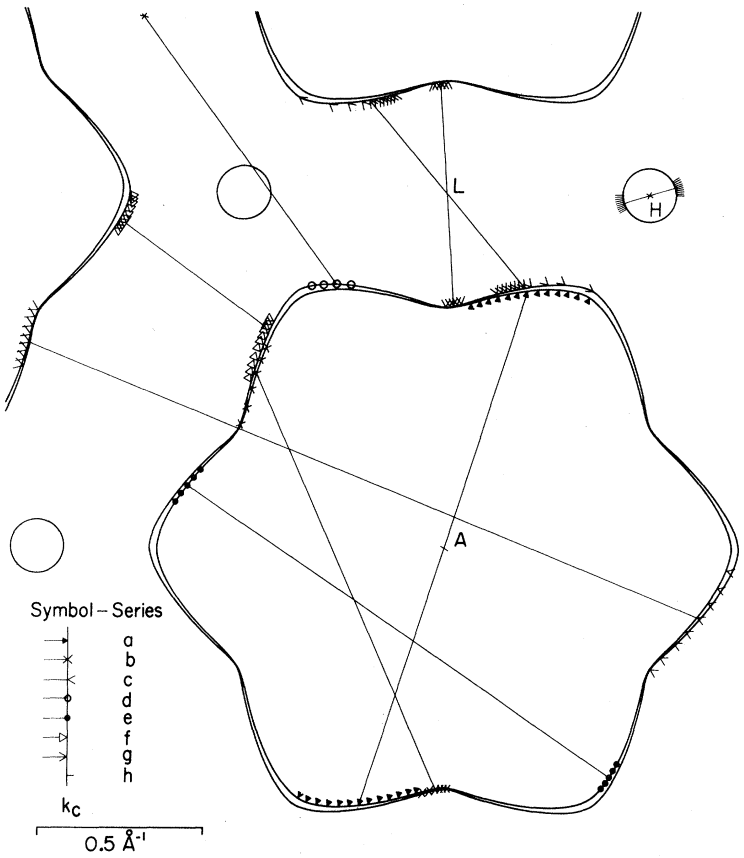

FIG. 4. Projection of the FS of Tl onto the *ALH* plane with the assignment of extremal calipers for $\vec{n}$ parallel to [0001].

is, to a large extent, dependent upon the geometry of the orbit. That is, extremal orbits that spend proportionately longer time in the skin depth of the sample, and whose trajectories are parallel to the surface while in the skin depth, have a greater effect on the surface impedance than do extremal orbits calipered at more pointed segments of the FS. An example of this fact is that the most intense signal observed in this investigation was series *o* between 9° and 15° from the $[10\bar{1}0]$ direction. Within this angular range, the signals due to this orbit had a signal-to-noise ratio of more than 1000 to 1. As can be seen in Figs. 4 and 6, it is in this region that the extremal orbits associated with these calipers have a flat and extensive trajectory in the skin depth of the sample. Another example in the consideration of signal intensity as a check on caliper assignment is the assignment of series *p* and *q*. The intensity of RFSE peaks decreased with increased angle of the field from the [0001] direction very rapidly indicating that the FS associated with these series became more pointed with increased angle.

Series *s*, *t*, and *u* result from truncated orbits due to the protrusion of the major peaks in the *ALM* plane above the main body of the third-band hole surface (Fig. 6). Calculated values of the central and noncentral dHvA areas for this cross section are given in Table III.

For *n* parallel to $[10\bar{1}0]$, only two series θ and ξ, with relatively weak signals, were assigned to closed central orbits on the third-band surface. The reason for the lack of observable central orbits in this orientation is that they must pass through the point of degeneracy between the third- and fourth-band surfaces at least twice during one orbit. That is, the number of electronic carriers spanning the third-zone hole surface on central orbits is diminished because of some of the carriers switching to orbits on the fourth zone as a result of magnetic breakdown near the point of degeneracy. Although series ξ is due to central orbits on a pointed section of the FS, it is observable since there are no other calipers in this region of magnetic field and angle. Orbits associated with caliper series θ contain a relatively large number of carriers, since for a given k_c there exists a large range of values for k_H having the same value of k_c. Thus, orbits contributing to the change in surface impedance resulting in this observed caliper series do not all pass through the degeneracy point.

Series π (Fig. 5) is additional evidence for the assignment of series *o* and *p* and indicates that

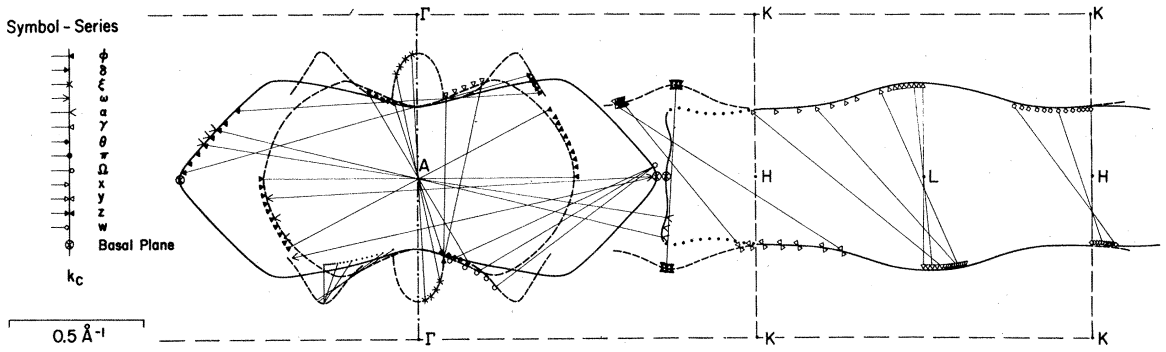

FIG. 5. Projection of the FS of Tl onto the *AHK* plane with the assignment of extremal calipers for $\vec{n}$ parallel to $[10\bar{1}0]$.

the third-band surface has a maximum extent of approximately 0.25 Å^{-1} along the $A\Gamma$ line. The assignment of the remaining series Ω, γ, and ζ (Fig. 5) allows a dHvA area for this cross section of the third-band surface to be calculated from scaled drawings and is in excellent agreement with previous experiments (Table III).

B. Fourth-Band Electrons

In all three orientations, the RFSE lines corresponding to extremal closed orbits on the fourth-band hexagonal network arms were very intense, indicating that these segments of the FS are relatively smooth and cylindrical. The outline of this network in the *ALH* plane is shown in Fig. 4. Caliper series *f* is due to a noncentral closed minimal orbit around the arms. It is consistent with the plots of series *g* and *d*, which have been interpreted as the result of closed maximal and minimal orbits on the electron surface (Fig. 4). Both of these calipers have their midpoint at the *L* point in the BZ. The dHvA area of closed orbits in the *ALH* plane on the inside of the fourth-band electron-ring network was computed directly from these data and is compared with previous experiments in Table III.

Series *k* and *l* (Fig. 6) result from maximal closed orbits on the fourth-band network. The outline shown in Fig. 6 due to calipers of these orbits is a projection of their extent onto the *ALM* plane and not a true cross section. Series *m* is due to a closed-hole orbit on the inside of the network, while series *j* is due to a minimal closed orbit at the junction of the arms.

Series *w*, *x*, and *y* are noncentral, closed, maximal, and minimal calipers which have been plotted self-consistently to give the outline shown in Fig. 5. Series *z* is designated as calipers from truncated orbits on the fourth-zone electron surface. However, this caliper series could also be interpreted as arising from maximal orbits on the third-zone hole surface passing over the top of the minor protrusions in the *AHK* plane. These calipers furnish a picture of the projection of the network onto the *AHK* plane. Caliper series *y* is a result of closed minimal orbits which are Y shaped when viewed along the *HK* direction. These orbits pass under one arm of the network and over the top of the two adjacent arms. Caliper series α arises from orbits starting on the third zone passing through one of the degeneracy points onto the fourth zone, back through a second degeneracy point, and completing the orbit on the third zone. When the predetermined outline of the third zone in the *AHK* plane (series δ) is used as one end of the caliper, and when the condition is imposed that the caliper pass through the degeneracy point, the other end of the caliper gives

TABLE III. Comparison of experimental dHvA areas.

Field direction	Band no.	Present data	Experimental area in Å^{-2}		Priestley[c]
			Ishizawa[a]	Anderson[b]	
0001	3	1.96	1.95	1.95	1.96
$10\bar{1}0$	3	0.943	0.936		0.936
$11\bar{2}0$	3 (central)	0.961			
$11\bar{2}0$	3 (noncentral)	0.900[d]	0.889	~0.889	0.876
0001	4	2.01	2.02	2.02	2.04
0001	5	~0.018	~0.019	~0.019	

[a]Ishizawa and W. R. Datars (Ref. 15).
[b]J. R. Anderson *et al.* (Ref. 14).
[c]M. G. Priestley (Ref. 12).
[d]Shown in Fig. 5 by dot-dashed line.

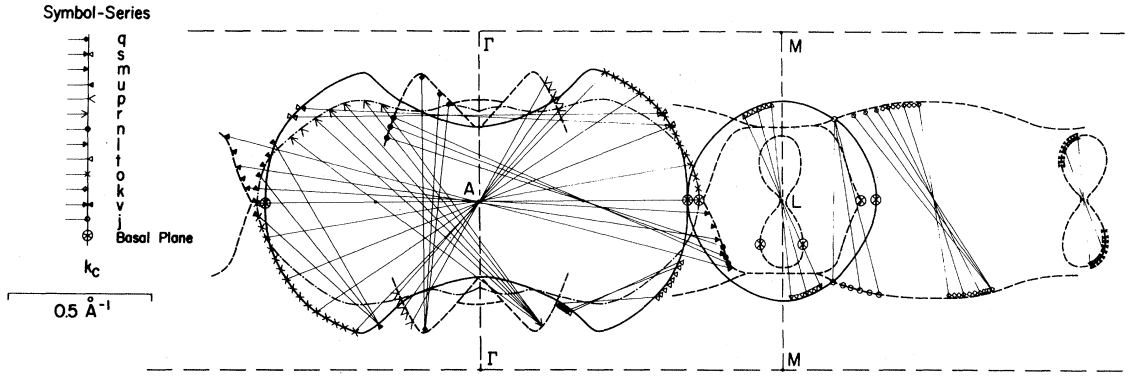

FIG. 6. Projection of the FS of Tl onto the *ALM* plane with the assignment of extremal calipers for $\hat{n}$ parallel to $[11\bar{2}0]$.

the cross section of the fourth zone in the *AHK* plane.[23] No orbits passing completely around the ring network were observed in this orientation because of the degeneracies along *AL* between the third- and fourth-band surfaces and the resulting switching between bands that occurs at these points.

The absence of the high extent of the three posts occurring on the fourth zone in the *AHK* plane in both the single-OPW and the ROPW models is clearly indicated by the assignment of series *x*, *y*, *w*, *k*, *j*, and *l*. In addition to this investigation, recent dHvA experiments[15] fail to show any evidence supporting the existence of the posts predicted by the ROPW and single-OPW models.

Series *i* is tentatively assigned as resulting from electronic carriers whose trajectories are nearly parallel to the sample surface as they pass through the skin depth on both sides of the sample. As can be seen in Fig. 6, orbits around the fourth-band arms could result in carriers running parallel to the $A\Gamma$ direction over a large part of this orbit. Since the cross section of these arms varies greatly as a function of distance from the *ALM* plane, it is not possible to definitely assign the position of series *i* in Fig. 4.

C. Fifth-Band Electrons

Series *v* and *h* are assigned to pockets of fifth-band electrons centered at *H*. Series *v* shows signs of splitting into two series as the angle of the field is rotated away from the $[10\bar{1}0]$; however, the signal strength becomes extremely weak as the angle is changed and is lost in the background at the lower fields. This indicates that more than one extremal orbit can exist on this portion of the surface. Effects of orbits similar to those responsible for series *v* were seen in the data taken on samples with $\hat{n}$ parallel to $[10\bar{1}0]$. However, calipers could not be assigned because the signals associated with series *w* interfered with the weaker RFSE lines of the fifth band. Both series *v* and *h* agree very well with the model proposed in Ref. 15 (Figs. 4 and 6). In Fig. 4 the outline of the surface is represented as essentially round. This construction is not unique, and the data could as easily be fitted to a triangular shape using noncentral orbits. In addition, the data show some deviation from a constant caliper which is not noticeable on the scale of Fig. 6.

V. CONCLUSION

In Table I a comparison between the FS calipers along the principal symmetry directions obtained in the present investigation and those of past experiments is given. In addition to the experimental values, calipers resulting from the single-OPW and Soven's ROPW calculations are given. Although there is little numerical agreement between experiment and theory, Soven's model accurately predicts the shape of the FS in the *ALH* plane. The primary topological differences between the present model and the FS predicted by the ROPW calculation are the reduction of fourth-zone posts in the *AHK* plane and the position and magnitude of the third-zone projections in the $A\Gamma$ direction. The ROPW model of the third-band hole surface has 12

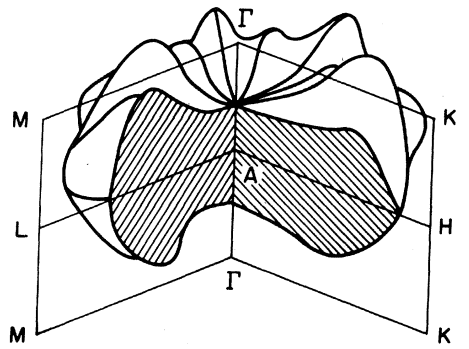

FIG. 7. Third-band hole surface derived from this investigation.

projections in the $A\Gamma$ direction of equal extension, with 3-m symmetry in planes 15° from the *ALM* and *AHK* planes. The model resulting from the present investigation (Fig. 7) has six minor projections in the *AHK* planes and six major ones in the *ALM* planes. Calipers assigned to the fifth-band pockets at *H* are in excellent agreement with a recently proposed model by Ishizawa and Datars.[13] This pocket of electrons shows the expected effect of spin-orbit coupling in the *AH* direction (Fig. 6). No calipers were observed that could be interpreted as resulting from orbits on third- or fourth-band pockets of the FS in the ΓMK plane. Also, no effects due to the proposed sixth-band electron pockets centered at *H* were seen. However, the present investigation does not exclude the presence of these segments of the FS. The relatively short mean free path at the higher temperatures necessary to avoid the superconducting phase in Tl results in very weak signals. The weak signals and the large slope in the surface impedance at low fields are possible explanations for the absence of calipers for these small pieces of the FS.

Calipers obtained in the present investigation are currently being used to adjust the nonlocal and spin-orbit coupling parameters occurring in a pseudopotential calculation of the energy bands for Tl.

ACKNOWLEDGMENTS

The authors are indebted to Professor C. G. Grenier for many informative discussions. The financial assistance received for the preparation of this manuscript from the Dr. Charles E. Coates Memorial Fund of the Louisiana State University Foundation donated by George H. Coates is gratefully acknowledged.

---

*Work supported by the National Science Foundation under Grant No. GP-11008.

[1]N. E. Alekseevskii and Yu. P. Gaidukov, Zh. Eksperim. i Teor. Fiz. 43, 2094 (1962) [Sov. Phys. JETP 16, 1481 (1963)].

[2]A. R. Mackintosh, L. E. Spanel, and R. C. Young, Phys. Rev. Letters 10, 434 (1963).

[3]J. C. Milliken and R. C. Young, Phys. Rev. 148, 558 (1966).

[4]R. C. Young, Phys. Rev. 163, 676 (1967).

[5]R. E. Hamburg, C. G. Grenier, and J. M. Reynolds, Phys. Rev. Letters 23, 236 (1969).

[6]J. A. Rayne, Phys. Rev. 131, 653 (1963).

[7]Y. Eckstein, J. B. Ketterson, and M. G. Priestley, Phys. Rev. 148, 586 (1966).

[8]J. B. Coon, C. G. Grenier, and J. M. Reynolds, J. Phys. Chem. Solids 28, 301 (1967).

[9]W. L. Dahlquist and R. G. Goodrich, Phys. Rev. 164, 944 (1967).

[10]J. C. Shaw and G. E. Everett, Phys. Rev. B 1, 537 (1970).

[11]D. Shoenberg, Phil. Trans. Roy. Soc. (London) A245, 1 (1952).

[12]M. G. Priestley, Phys. Rev. 148, 580 (1966).

[13]Y. Ishizawa and W. R. Datars, Phys. Letters 30A, 463 (1969).

[14]J. R. Anderson, J. E. Schirber, and D. R. Stone, Colloque International sur les Propriétés Physiques des Solides sous Pression, Grenoble, 1969 (unpublished).

[15]Y. Ishizawa and W. R. Datars, Phys. Rev. B (to be published).

[16]P. Soven, Phys. Rev. 137, A1717 (1965).

[17]R. C. Jones, R. G. Goodrich, and L. M. Falicov, Phys. Rev. 174, 672 (1968).

[18]O. L. Steenhaut and R. G. Goodrich, Phys. Rev. B 1, 4511 (1970).

[19]G. E. Juras, Phys. Rev. B 2, 2869 (1970).

[20]D. A. Boudreau and R. G. Goodrich, Phys. Rev. B (to be published).

[21]V. F. Gantmakher and I. P. Krylov, Zh. Eksperim. i Teor. Fiz. 49, 1054 (1965)[Sov. Phys. JETP 22, 734 (1966)].

[22]M. H. Cohen and L. M. Falicov, Phys. Rev. 130, 92 (1962).

[23]An alternative assignment of this series would be similar to its present assignment, but passing through a different set of degeneracy points. However, if this is done, the fourth zone in the *AHK* plane has a maximum extent in this plane extending in an almost straight line from the *AL* line to the *LK* line. This alternative assignment would make the assignments of series *z* and *m* topologically inconsistent. When the outline of the fourth zone in Fig. 6 is projected onto Fig. 5, it more nearly agrees with the outline in Fig. 5 as given and in addition, the *z* series assignment would be an open orbit with this alternative. The authors are indebted to Professor C. G. Grenier for pointing out the consequences of these two alternatives to them.